Accepted Manuscript

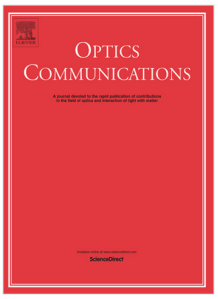

Cooperative Up-converted luminescence in Yb,Na:CaF_2 cladding waveguides by femtosecond laser inscription

Limu Zhang, Taiyong Guo, Yingying Ren, Yangjian Cai, Mark D. Mackenzie, Ajoy K. Kar, Yicun Yao

PII: S0030-4018(19)30040-9
DOI: https://doi.org/10.1016/j.optcom.2019.01.032
Reference: OPTICS 23792

To appear in: *Optics Communications*

Received date : 5 December 2018
Revised date : 9 January 2019
Accepted date : 12 January 2019

Please cite this article as: L. Zhang, T. Guo, Y. Ren et al., Cooperative Up-converted luminescence in Yb,Na:CaF_2 cladding waveguides by femtosecond laser inscription, *Optics Communications* (2019), https://doi.org/10.1016/j.optcom.2019.01.032

1. Cladding waveguides are fabricated in Yb,Na:CaF_2 by femtosecond laser inscription.
2. Low propagation losses and single-mode waveguides are obtained.
3. Modification mechanism is revealed by investigating the confocal μ-Raman properties.
4. Visible cooperative up-conversion emissions are achieved in the waveguides.

Cooperative Up-converted Luminescence in Yb,Na:CaF_2 Cladding Waveguides by Femtosecond Laser Inscription

Limu Zhang[a], Taiyong Guo[a], Yingying Ren[a*], Yangjian Cai[a], Mark D. Mackenzie[b], Ajoy K. Kar[b], Yicun Yao[c]**

[a]*Center of Light Manipulations and Applications & Shandong Provincial Key Laboratory of Optics and Photonic Device, School of Physics and Electronics, Shandong Normal University, Jinan 250014, China*

[b]*Institute of Photonics and Quantum Sciences, Heriot-Watt University, Edinburgh EH14 4AS, UK*

[c]*School of Physics Science and Information Technology, Liaocheng University, Liaocheng 252059, China*

[*]*Corresponding author: ryywly@sdnu.edu.cn*

[**]*Corresponding author: yangjiancai@sdnu.edu.cn*

Abstract: Cladding waveguides are fabricated in Yb,Na:CaF_2 crystal by applying femtosecond laser inscription. Waveguide properties are investigated in terms of guiding behaviors and confocal micro-Raman characterizations. In addition, under 946 nm excitation, visible cooperative up-conversion emissions at 478 nm induced by Yb^{3+} ion pairs are observed while other visible bands are detected owing to the impurities of Er^{3+} and Tm^{3+} ions.

Keywords: Femtosecond laser inscription, Cladding waveguides, Cooperative up-conversion, Yb,Na:CaF_2 crystal.

1. Introduction

Femtosecond laser inscription (FLI) has been proved to be an effective technology for optical waveguide fabrication in numerous optical materials [1-4]. Waveguide structure with a tubular cladding morphology, a central unexposed waveguide core surrounded by laser induced low-index tracks, have attracted increasing attention mainly because such structures can be tailored according to demand and the properties of the host materials can be preserved well in the guiding regions [5-7]. Compact lab-on-chip devices based on cladding waveguide structures have been achieved including beam couplers or splitters, novel waveguide lasers and frequency converters [8-13].

CaF_2 crystal shows unique advantages when compared with other fluoride materials. It has wide transmission band ranging from deep ultraviolet to mid-infrared;

it also has low refractive index and nonlinear coefficient, which can reduce the nonlinear effect of high-intensity laser pumping; It exhibits lower phonon energy that can improve the quantum efficiency of fluorescence and result in relatively low lasing threshold. It also possesses a high laser damage threshold [12-18]. All these properties make CaF_2 crystal an important doping substrate for various optical applications. The Yb^{3+} ion shows a very simple electronic level structure with the ground state ($^2F_{7/2}$) and an excited state ($^2F_{5/2}$), leading to puny shielded 4f electrons, which makes Yb^{3+} ions easy to interact with the lattice and neighbor ions. In consequence, so called cooperative up-conversion in visible blue regions, produced by two nearby-located Yb^{3+} ions, can be observed in Yb-doped materials [19-31]. Therefore, Yb:CaF_2 crystal is considered to be an excellent candidate for visible luminescence generation. However, it has been demonstrated that the advantages of Yb:CaF_2 are often mitigated by the formation of Yb^{2+}-ions and the ion clusters. An effective solution is to introduce non-active ions (such as Na^+) into rare-earth doped CaF_2 crystal [12,32]. Visible luminescence devices based on cladding waveguides in Yb,Na:CaF_2 crystal, which combine the compact geometries of guiding structures while maintaining the advantages of the substrate material, show promising potential for applications in information technology, color display, biomedical diagnostics and underwater optical communication [33-36]. In this work, we demonstrate the formation and up-conversion of cladding waveguides in Yb,Na:CaF_2 crystal by using FLI. The guiding performance of the waveguides are observed to be excellent. By observing the micro-Raman characterizations, the mechanism of the waveguides formation is revealed. More importantly, visible blue up-conversion of Yb^{3+} ions at 478 nm based on cooperative transition in the guiding regions are reported. Extra fluorescence bands in the violet, blue, green and red regions are also detected which are due to Er^{3+} and Tm^{3+} ion impurities.

2. Experimental Procedures

The 2.0 at% Yb^{3+}-ions and 5.0 at% Na^+-ions are incorporated into CaF_2 cubic crystal which is cut into a size of 2 mm × 10 mm × 10 mm and then optically polished. The tubular cladding structures are fabricated in the prepared Yb,Na:CaF_2 crystal by applying FLI. During the fabrication process, an ultrafast Yb-doped fiber master-oscillator power amplifier laser (IMRA FCPA μ-Jewel D400) is used as laser source, delivering 360 fs pulses with a repetition rate of 500 KHz and a center

wavelength of 1047 nm. The laser beam with circular polarization is focused by a microscope objective (NA=0.4) into the substrate beneath one of the 10 × 10 mm^2 surfaces. The sample is translated through the focused laser at a speed of 20 mm/s. The inscription power of laser beam is varied from 100 mW to 160 mW with a step of 20 mW, corresponding to pulse energys varied from 200 nJ to 320 nJ with a step of 40 nJ. Under these conditions, arrays of parallel tracks are inscribed below the top surface following the designed geometries so as to form claddings waveguides with diameters ranging from 20 μm to 35 μm. The central depths of these cladding structures are positioned around 100 μm below the sample surface. In order to enhance the refractive index (RI) contrast of waveguiding core compared with laser-induced tracks, the scanning process is repeated with different numbers of overlapping scans (3 scans or 10 scans) for each track. Consequently, 32 cladding waveguides (numbered as WG1-WG32) are fabricated.

By using a linearly-polarized diode laser at 633 nm and end-face coupling, experiments are carried out to illustrate the guiding characteristics of the waveguides. A half-wave plate is employed to control the polarizations of the incident laser. Modal profiles of these structures are detected. The RI contrast Δn is calculated roughly by the formula [37]:

$$\Delta n = \frac{\sin^2\theta_m}{2n_s} \tag{1}$$

in which θ_m is the maximum permitted incident angle. Propagation losses are estimated by detecting the incident and output power while taking Fresnel reflection of the end facets and the coupling efficiency into account. The propagation loss α can be estimated with the following equation [38]:

$$P_{out} = P_{in} \cdot (1 - R)^2 \cdot e^{-\alpha L} \cdot T \tag{2}$$

where R is the Fresnel reflection coefficient, which is calculated to be 0.0318. L stands for the length of the waveguide. T is related to the mismatch between the pump beam mode and waveguide mode which, for single-mode waveguides, can be expressed as [38]:

$$T = \left(\frac{2\omega_1\omega_2}{\omega_1^2+\omega_2^2}\right)^2 \tag{3}$$

where ω_1 and ω_2 are the mode width of waveguide and pump beam，respectively. Presuming single-mode guidance for all waveguides, the values of T are estimated to be 0.934, 0.988, 0.995 and 0.917 for the waveguides with diameters of 35 μm, 30 μm,

25 μm and 20 μm, respectively. It should be pointed out that, for multi-mode waveguides, the values of parameters related to the mode mismatch are larger than the calculated results of T due to the mode transition. Thus, the propagation losses of multi-mode waveguides should be smaller than the calculated values.

The confocal Raman properties of the cladding waveguide WG1 are further investigated with a fiber-coupled confocal microscope (alpha300 R, WITec GmBH). The excitation laser is a diode-pumped solid-state laser (532 nm, Cobalt Laser). The continuous wave laser is focused via a 50× objective (NA = 0.55). The lateral and axial resolutions of the confocal system are 500 nm and 1 um, respectively. The Raman scattered light are dispersed by a 600 mm focal length spectrometer with 1800 grooves/mm grating (UHTS 600). The signals are eventually detected using a charge-coupled-device (CCD) thermoelectrically cooled to -60 °C. In order to obtain the in-depth variation of the Raman spectra, the excitation spot is scanned continuously over the cross section of WG1 with the emission line at 321 cm^{-1}. Two dimensional (2D) mappings including the emitted intensity, peak position of the emission line and emission bandwidth are obtained. Meanwhile, for easy visualization and comparison, 1D profiles of micro-Raman are also detected.

Additionally, based on the end-face coupling system, the experiment for up-conversion emission is actualized by using a 946 nm diode-pumped solide-state laser as excitation laser. The linearly polarized beam is focused and coupled into the waveguide in combination with a dielectric mirror which has high transmittance at around 946 nm in order to increase the pump power incident into the waveguide. A half-wave plate is used so as to investigate fluorescence properties in both of the two polarizations. After being separated from the residual pump with a 900 nm short pass filter, the up-conversion emissions from the waveguides and, for comparison, from the bulk are detected.

3. Results and Discussion

The fabricating parameters of 32 WGs are shown in Table 1, where the experimentally obtained mode profile patterns at wavelength of 633 nm are also depicted. These waveguides are capable of supporting both TE and TM polarizations, and the mode distributions did not exhibit significant difference, which underlines the advantage of polarization independence of the cladding structures owing to their symmetric morphologies. Strong optical confinements are obtained from all

waveguides and the mode distributions of WG1-WG4 have been reported elsewhere [39]. Single-mode guidance is obtained from structures with a diameter of 20 μm, revealing that mode numbers are reduced along with the reduction of the waveguide diameters. Furthermore, some waveguides (WG14, WG15, WG27, WG30 and WG31), although possessing larger diameter, are also single-mode which is related to the smaller RI contrasts induced by relatively low inscription powers when compare to those produced with high laser powers. Furthermore, the single-mode performance of cladding waveguide WG27 indicates lower RI contrast of waveguides fabricated with 3 scans than those fabricated with 10 scans. Such a result is also numerically proved by calculating the values of RI contrast of these waveguides (see below).

Figure 1(a) shows the cross-sections of WG1 and WG17 where it can be clearly seen that the laser-induced damage only occurs at the modified areas, forming distinct waveguide boundaries deeply embedded inside the sample, while the core regions and the bulk outside the claddings are without any obvious damages. The propagation losses of cladding waveguides (10 scans) obtained under TM and TE polarization are plotted in Fig. 1(b). The minimum value is estimated to be around 0.5 dB/cm for WG1. It can be seen clearly that, at fixed inscription power, reduced propagation losses are obtained when the guiding cores are enlarged. Meanwhile, for waveguides with the same diameter, the propagation losses decrease monotonously when the irradiated-laser power increasing from 100 mW to 160 mW. Fig. 1(c) shows the RI contrast of waveguides with 10 scans. It can be obtained that, the waveguides fabricated with 100 mW laser power possess minimum RI contrast around 1.0×10^{-3} and the waveguides inscribed with 120 mW, 140 mW and 160 mW have similar RI contrast (from 1.3×10^{-3} to 1.4×10^{-3}). For waveguides with 3 scans, very similar variation trends of propagation losses and RI contrasts are observed. Meanwhile, higher guiding losses related to lower RI contrast of waveguides with 3 scans are obtained when compared with corresponding waveguides of 10 scans. The lowest guiding loss is realized in WG17 with a value of approximately 0.6 dB/cm and the maximum RI variation of around 1.2×10^{-3} is obtained. It can be clearly observed that negligible differences are observed for TE and TM polarizations.

Figure 2(a) illustrates the micro-Raman emission lines obtained from the waveguide area (point A as indicated in Fig. 2(b)) and a laser-induced track (point B) of WG1. As can be seen, the micro-Raman intensity inside the track suffers from a strong quenching. In order to get complete knowledge on the spatial distributions of

the changes in the micro-Raman spectra, and hence on the corresponding microstructural changes over the whole waveguide cross-section, the spatial distribution of the intensity, spectral shift and bandwidth of the emission line are measured in 2D (as shown in Figs. 2(b)-2(d)) and 1D (Figs. 2(e)-2(g)) forms. 1D profiles are measured along the green lines crossing the waveguide indicated in Figs. 2(b)-2(d). As can be seen from these figures, obvious reductions in Raman intensity, blue shifts and broadening of the emission line are spatially located at the modified volumes. These phenomena, in general, can be attributed to the creation of lattice defects and damages in these regions, which are responsible for the RI reduction in the cladding areas. Furthermore, Figs. 2(b)-2(g) also demonstrate that in the active volume of the waveguide similar Raman intensity, peak position and band width are obtained in respect to bulk, which, in general, means that the lattice structures in the guiding areas are well preserved during the FLI procedure so that good optical properties of substrate material can be expected in the waveguide cores.

Figure 3(a) depicts the up-conversion emission spectra collected from the cladding waveguides (WG1-WG17) and the bulk, which are realized under 946 nm at room temperature with fixed excitation power. As can be seen from Fig. 3(a), the up-conversion performance improved obviously when the inscription power is increased and the guiding core is enlarged due to the reduction of propagation losses. The best performance is observed in WG1. For 3 scans, the best up-conversion emission is realized in WG17 as shown in Fig. 3(a), and the intensity of the emission is much lower than that obtained in WG1. Meanwhile, in comparison with the bulk, the emission intensities are strengthened in the waveguides, which reveals the strong optical confinement of the fluorescence emission in the guiding volumes, making these waveguides promising for integrated fluorescence devices. Further evidence can be found from the photographs of visible up-conversion emissions observed in WG1 and bulk area, as exhibited in Figs. 3(b) and (c), from which a clear intensity quenching in the bulk is observed.

To investigate the details of the guided up-conversion emission, the spectra of the fluorescence generated from WG1 is measured, as described in Fig. 4. As it can be seen, an overall increase in the intensity of all the emission lines is observed when the excitation power is increased. The emission spectra show broad band covering blue-violet, blue, green and red regions, which, in a first order approximation, can be attributed to the impurities of Er^{3+}, Tm^{3+} or other rare earths in Yb^{3+} doped substrate

since it is hard to separate the Ln^{3+} ions due to their similar chemical properties. Such phenomena have been previously demonstrated in materials such as Yb:YAG waveguide [26] and Yb:$Lu_3Sc_2Ga_3O_{12}$ nano-garnets [22]. The peaks observed around 408 nm and 545 nm are associated with the Er^{3+} ions transitions corresponding to ($^2H_{9/2}$,$^4S_{3/2}$)→$^4I_{15/2}$, respectively. The transitions $^4F_{9/2}$→$^4I_{15/2}$ of Er^{3+} ions and $^1G_4$→$^3F_4$ of Tm^{3+} ions cause the red band with center of 657 nm [40-43]. It is found that, although the concentrations of Er^{3+}, Tm^{3+} are low, the intensities of emission lines around 657 nm are quite strong. This is mainly because the up-conversion luminescence of the impurity ions are induced by energy transfer from the Yb^{3+} ions to Er^{3+} and Tm^{3+}, which have been proved to possess very high efficiency [44]. Emission line centered at 478 nm is induced by up-conversion process of Yb^{3+} ions pairs and Tm^{3+} ($^1G_4$→$^3H_6$). However, the generation of this peak is dominated by cooperative up-conversion emission, which can be confirmed by several evidences. Firstly, cooperative emission has been reported previously in Yb^{3+} doped materials [22-31]. Such a phenomenon can be explained in terms of the radiative relaxation of the simultaneously excited Yb^{3+} ion pairs accompanied by the emission of a visible photon with the sum of energies, which can be expressed as $^2F_{5/2} + {}^2F_{5/2} \rightarrow 2^2F_{7/2} + h\nu$. [45,46] Secondly, the cooperative emission shows fairly wide band which has never been observed in up-conversion luminescence of other rare earth ions [20,47]. Finally, it has been proved that, for the up-conversion of Tm^{3+}, the emission lines around 800 nm (corresponding to the transition from $^3H_4$ to $^3H_6$) have much stronger intensity than that induced by transition of $^1G_4$→$^3H_6$. However, in our work, the peak around 800 nm is relatively low, which in turn, proves that the emission intensity of Tm^{3+} from $^1G_4$ to $^3H_6$ is very weak [48,49]. Consequently, it can be concluded that the energy band corresponding to 478 nm is mainly attributed to cooperative up-conversion of Yb^{3+} pairs.

4. Conclusion

Cladding waveguides in Yb,Na:CaF_2 crystal are fabricated by FLI with various parameters. With optimized inscription conditions, the fabricated structures show good guiding performance in terms of low propagation losses, single-mode guidance and polarization independence. The micro-Raman characterizations reveal that laser-induced lattice defects only occur on tracks while properties of the bulk are well

preserved in guiding volumes. Under 946 nm excitation, the visible cooperative up-conversion emissions of Yb^{3+} ion pairs at 478 nm are achieved in the waveguides while energy transfers from Yb^{3+} ions to Er^{3+} and Tm^{3+} impurities are responsible for the other bands of emission spectra. These cladding waveguides show good potential for integrated optical circuits and miniature visible fluorescence waveguide devices.

Acknowledgments

This work is supported by the National Natural Science Foundation of China under Grant Nos. 11404194 and 11874243, Shandong Natural Science Foundation (ZR2016AB03) and Shandong Science Research Program for Universities (J16LJ08).

References

1. F. Chen, J.R.V. de Aldana, Optical waveguides in crystalline dielectric materials produced by femtosecond laser micromachining, Laser Photonics Rev. 8 (2014) 251-275.
2. Y.L. Zhang, Q.D. Chen, H. Xia, H.B. Sun, Designable 3D nanofabrication by femtosecond laser direct writing, Nano Today 5 (2010) 435-448.
3. D. Choudhury, J.R. Macdonald, A.K. Kar, Ultrafast laser inscription: perspectives on future integrated applications, Laser Photonics Rev. 8 (2014) 827-846.
4. Y. Tan, F. Chen, J.R.V. de Aldana, G.A. Torchia, A. Benayas, D. Jaque, Continuous wave laser generation at 1064 nm in femtosecond laser inscribed Nd:YVO_4 channel waveguides, Appl. Phys. Lett. 97 (2010) 0311191-0311193.
5. H.L. Liu, Y.C. Jia, J.R.V. de Aldana, D. Jaque, F. Chen, Femtosecond laser inscribed cladding waveguides in Nd:YAG ceramics: Fabrication, fluorescence imaging and laser performance, Opt. Express 20 (2012) 18620-18629.
6. Y.Y. Ren, L.M. Zhang, H.G. Xing, C. Romero, J.R.V. de Aldana, F. Chen, Cladding waveguide splitters fabricated by femtosecond laser inscription in Ti:Sapphire crystal, Opt. Laser Techno. 103 (2018) 82-88.
7. H.L. Liu, S.Y. Luo, B. Xu, H.Y. Xu, Z.P. Cai, M.H. Hong, P.F. Wu, Femtosecond-laser micromachined Pr:YLF depressed cladding waveguide: Raman, fluorescence, and laser performance, Opt. Mater. Express 7 (2017) 3990-3997.
8. C. Chen, H.L. Liu, Y. Tan, J.R.V. de Aldana, F. Chen, Passively Q-switched waveguide lasers based on two-dimensional transition metal diselenide, Opt. Express 24 (2016) 10385-10390.
9. A.G. Okhrimchuk, A.V. Shestakov, I. Khrushchev, J. Mitchell, Depressed cladding, buried waveguide laser formed in a YAG:Nd^{3+} crystal by femtosecond laser writing, Opt. Lett. 30 (2005) 2248-2250.
10. Y.Y. Ren, L.M. Zhang, J.M. Lv, Y.F. Zhao, C. Romero, J.R.V. de Aldana, F. Chen, Optical-lattice-like waveguide structures in Ti:Sapphire by femtosecond laser inscription for beam splitting, Opt. Mater. Express 7 (2017) 1942-1949.

11. Y. Tan, Q.F. Luan, F.Q. Liu, S. Akhmadaliev, S.Q. Zhou, F. Chen, Swift carbon ion irradiated Nd:YAG ceramic optical waveguide amplifier, Opt. Express 21 (2013) 13992-13997.
12. H.L. Liu, Y. Tan, J. R. Vázquez de Aldana, F. Chen, Efficient laser emission from cladding waveguide inscribed in Nd:$GdVO_4$ crystal by direct femtosecond laser writing, Opt. Lett. 39 (2014) 553-556.
13. H.L. Liu, J. R. Vázquez de Aldana, M.H. Hong, F. Chen, Femtosecond laser inscribed Y-branch waveguide in Nd:YAG crystal: fabrication and continuous-wave lasing, IEEE J. Sel. Top. Quant. Electronics 22 (2015) 227-230.
14. L.B. Su, J. Xu, H.J. Li, W.Q. Yang, Z.W. Zhao, J.L. Si, Y.J. Dong G.Q. Zhou, Codoping Na^+ to modulate the spectroscopy and photoluminescence properties of Yb^{3+} in CaF_2 laser crystal, Opt. Lett. 30 (2005) 1003-1005.
15. J.L. Doualan, L.B. Su, G. Brasse, A. Benayad, V. Menard, Y.Y. Zhang, A. Braud, P. Camy, J. Xu, R. Moncorgé, Improvement of infrared laser properties of Nd:CaF_2 crystals via codoping with Y^{3+} and Lu^{3+} buffer ions, J. Opt. Soc. Am. B 30 (2013) 3018-3021.
16. G. Lakshminarayana, R. Yang, M.F. Mao, J.R. Qiu, I.V. Kityk, Photoluminescence of Sm^{3+}, Dy^{3+}, and Tm^{3+}-doped transparent glass ceramics containing CaF_2 nanocrystals, J. Non-Cryst. Solids 355 (2009) 2668-2673.
17. P. Cortelletti, M. Pedroni, F. Boschi, S. Pin, P. Ghigna, P. Canton, F. Vetrone, A. Speghini, Luminescence of Eu^{3+} Activated CaF_2 and SrF_2 Nanoparticles: Effect of the Particle Size and Codoping with Alkaline Ions, Cryst. Growth Des. 18 (2018) 686-694.
18. L.H. Zheng, L.B. Su, J. Xu, Growth and Characterization of Ytterbium Doped Silicate Crystals for Ultra-Fast Laser Applications, Modern Aspects of Bulk Crystal and Thin Film Preparation, InTech, 2012.
19. P. Klopp, New Yb^{3+}-doped laser materials and their application in continuous-wave and mode-locked lasers, Humboldt-Universität zu Berlin, Mathematisch-Naturwissenschaftliche Fakultät I, 2006.
20. N. Olliera, J.L. Doualan, V. Pukhkaya, T. Charpentier, R. Moncorgé, S. Sen, Evolution of Yb^{3+} environment and luminescence properties under ionizing irradiation in aluminoborosilicate glasses, J. Non-Cryst. Solids 357 (2011) 1037-1043.
21. Y.Z. Cheng, J.M. Lv, S. Akhmadaliev, I. Hernández-Palmero, C. Romero, J.R.V. de Aldana, Y. Tan, F. Chen, Optical ridge waveguides in Yb:YAG laser crystal produced by combination of swift carbon ion irradiation and femtosecond laser ablation, Opt. Laser Techno. 72 (2015) 100-103.
22. R. Praveena, P. Venkatalakshmamma, V. Sravani Sameer, V. Venkatramu, I.R. Martín, V. Lavín, C.K..Jayasankar, Near infrared and blue cooperative Yb^{3+} luminescence in $Lu_3Sc_2Ga_3O_{12}$ nano-garnets, Mater. Res. Bull. 101 (2018) 347-352.
23. S. Pramal, L. Steenhohle, W. Skorupa, Blue electroluminescence of ytterbium clusters in SiO_2 by cooperative up-conversion, Appl. Phys. B 98 (2010) 451-454.
24. V. Jubera, J. Sablayrolles, F. Guillen, R. Decourt, M. Couzi, A. Garcia, From the infrared to the visible range: Spectroscopic studies of ytterbium doped oxyborates, Opt. Commun. 282 (2009) 53-59.
25. X.F. Wang, S.G. Xiao, X.L. Yang, J.W. Ding, Highly efficient cooperative up-conversion of Yb^{3+} in $NaYF_4$, J. Mater. Sci. 43 (2008) 1354-1356.

26. G.V. Vázquez, H. Desirena, E. De la Rosa, E. Flores-Romero, H. Márquez, J. Rickards, R. Trejo-Luna, Upconversion emission in a carbon-implanted Yb:YAG planar waveguide, Opt. Commun. 285 (2012) 5531-5534.
27. Y. Le´vesque, S. Jandl, M. Bettinelli, Cooperative emission study in ytterbium doped $NaYO_4$, J. Lumin. 131 (2011) 1077-1081.
28. B.X. Jiang, Z.W. Zhao, X.D. Xu, P.X. Song, X.D. Wang, J. Xu, Visible luminescence in Yb^{3+}-doped gadolinium gallium garnets, Mater. Sci. Eng. B 137 (2007) 20-23.
29. B. Schaudel, P. Goldner, M. Prassas, F. Auzel, Cooperative luminescence as a probe of clustering in Yb^{3+} doped glasses, J. Alloys. Compd. 300-301 (2000) 443-449.
30. A.V. Kir'yanov, Y.O. Barmenkov, I.L. Martinez, Cooperative luminescence and absorption in Ytterbium-doped silica fiber and the fiber nonlinear transmission coefficient at λ=980 nm with a regard to the Ytterbium ion-pairs' effect, Opt. Express 14 (2006) 3981-3992.
31. X.B. Qiao, Y. Ye, Novel blue cooperative up-conversion luminescence of fully concentrated Yb-based $LiYb(MoO_4)_2$ phosphor, Mater. Lett. 161 (2015) 248-250.
32. J. Du, X.Y. Liang, Y.G. Wang, L.B. Su, W.W. Feng, E.Y. Dai, Z.Z. Xu, J. Xu, 1ps passively mode-locked laser operation of Na,Yb:CaF_2 crystal, Opt. Express 13 (2005) 7970-7975.
33. M. Kowalczyk, A. Major, J. Sotor, High peak power ultrafast Yb:CaF_2 oscillator pumped by a single-mode fiber-coupled laser diode, Opt. Express 25 (2017) 26290-26295.
34. J. Korner, J. Hein, H. Liebetrau, R. Seifert, [illegible] M. Kahle, M. Loeser, M. Siebold, U. Schramm, M.C. Kaluza, Efficient burst mode amplifier for ultra-short pulses based on cryogenically cooled Yb^{3+}:CaF_2, Opt. Express 21 (2013) 29006-29012.
35. V. Petit, P. Moretti, P. Camy, J.L. Doualan, F. Moncorg, Active waveguides produced in Yb^{3+}:CaF_2 by H^+ implantation for laser applications, J. Alloy. Compd. 451 (2008) 68-70.
36. L.B. Su, J. Xu, Y.H. Xue, C. Wang, L. Chai, X.D. Xu, G.J. Zhao, Low-threshold diode-pumped Yb^{3+},Na^+:CaF_2 self-Q-switched laser, Opt. Express 13 (2005) 5635-5640.
37. J. Siebenmorgen, K. Petermann, G. Huber, K. Rademaker, S. Nolte, A. Tunnermann, Femtosecond laser written stress-induced $Nd:Y_3Al_5O_{12}$ (Nd:YAG) channel waveguide laser, Appl. Phys. B 97 (2009) 251-255.
38. D. Marcuse, Loss Analysis of Single-Mode Fiber Splices, Bell. Syst. Tech. J. 56 (1997) 703-718.
39. Y.Y. Ren, C. Cheng, Y.C. Jia, Y. Jiao, D.W. Li, M.D. Mackenzie, A.K. Kar, F. Chen, Switchable single-dual wavelength Yb,Na:CaF_2 waveguide lasers operating in continuous-wave and pulsed regimes, Opt. Mater. Express 8 (2018) 1633-1641.
40. Y.J. Liu, Z.G. Song, C. Li, R. Wan, J.B. Qiu, Z.W. Yang, Z.Y. Yin, Y. Yang, X. Wang, Q. Wang, Efficient near-infrared to visible and ultraviolet upconversion in polycrystalline BiOCl:Er^{3+}/Yb^{3+} synthesized at low temperature, Ceram. Int. 39 (2013) 8911-8916.
41. Y. Dwivedi, S.B. Raiw, Blue and Red Luminescence from Europium-Doped Barium TetraBorate Crystals, J. Am. Ceram. Soc. 93 (2010) 727-731.
42. X.Q. Chen, Y.L. Li, F. Kong, L.P. Li, Q. Sun, F.P. Wang, Red, green, blue and bright white upconversion

luminescence of $CaTiO_3$: $Er^{3+}/Tm^{3+}/Yb^{3+}$ nanocrystals, J. J. Alloy. Compd. 541 (2012) 505-509.

43. Z.L. Fu, T.Q. Sheng, Z.J. Wu, Y.N. Yu, T. Cui, A novel and tunable upconversion luminescent material $GdPO_4$: Yb^{3+}, Ln^{3+} (Ln = Er, Tm, Ho), Mater. Res. Bull. 56 (2014) 138-142.
44. F. Auzel, P. Goldner, Towards rare-earth clustering control in doped glasses, Opt. Mater. 16 (2001) 93-103.
45. E. de la Rosa, P. Salas, L.A. Díaz-Torres, A. Martínez, C. Angeles, Strong Visible Cooperative Up-Conversion Emission in ZrO_2:Yb^{3+} Nanocrystals, J. Nanosci. Nanotechno. 5 (2005) 1480-1484.
46. X.H. Liu, W.H. Di, W.P. Qin. Cooperative luminescence mediated near-infrared photocatalysis of CaF_2:Yb@$BiVO_4$ composites, Appl. Catal. B: Environ 205 (2017) 158-164
47. M. Puchalska, E. Zych, A. Watras, Cooperative up-conversion processes in $SrAl_4O_7$:Yb and $SrAl_4O_7$:Yb,Tb and their dependence on charge compensation by Na, J. Lumin. 183 (2017) 185-192.
48. D.X. Wang, M. Nie, Z.G. Zhang, H. Li, L. Li, X.L. Zhang, X.W. Zhang, X.M. Ji, Intrinsic bistability effect of Yb-sensitized Tm upconversion emission in zirconium dioxide nanocrystal, Proc. of SPIE. 8335 (2012) 051-057.
49. G.Y. Chen, T.Y. Ohulchanskyy, R. Kumar, H. Ågren, P.N. Prasad, Ultrasmall Monodisperse $NaYF_4$:Yb^{3+}/Tm^{3+} Nanocrystals with Enhanced Near-Infrared to Near-Infrared Upconversion Photoluminescence, ACS. Nano 4 (2010) 3163-3168

Figure and Table captions

Figure 1. (a) The end-face microscope images of Yb,Na:CaF_2 cladding waveguides WG1 and WG17. (b) The propagation losses and (c) the refractive index contrast of waveguides with 10 scans obtained under TM and TE polarization.

Figure 2. (a) Raman spectra obtained from the guiding area and a damage track of WG1. The spatial distributions and 1D profiles of Raman intensity ((b) and (e)), Raman shift ((c) and (f)) and bandwidth ((d) and (g)) obtained from the cross-section of WG1. 1D profiles are detected along the green lines indicated in (b), (c) and (d).

Figure 3. (a) Up-conversion emissions of waveguides (WG1-WG17) and the bulk. The photographs of the visible fluorescence generated in WG1 (b) and the bulk (c).

Figure 4. Up-conversion spectra obtained from WG1 under the 946 nm excitation.

Table 1. Mode profiles observed from the fabricated 32 waveguides (WG1-WG32); MM and SM represent multi-mode and single-mode, respectively.

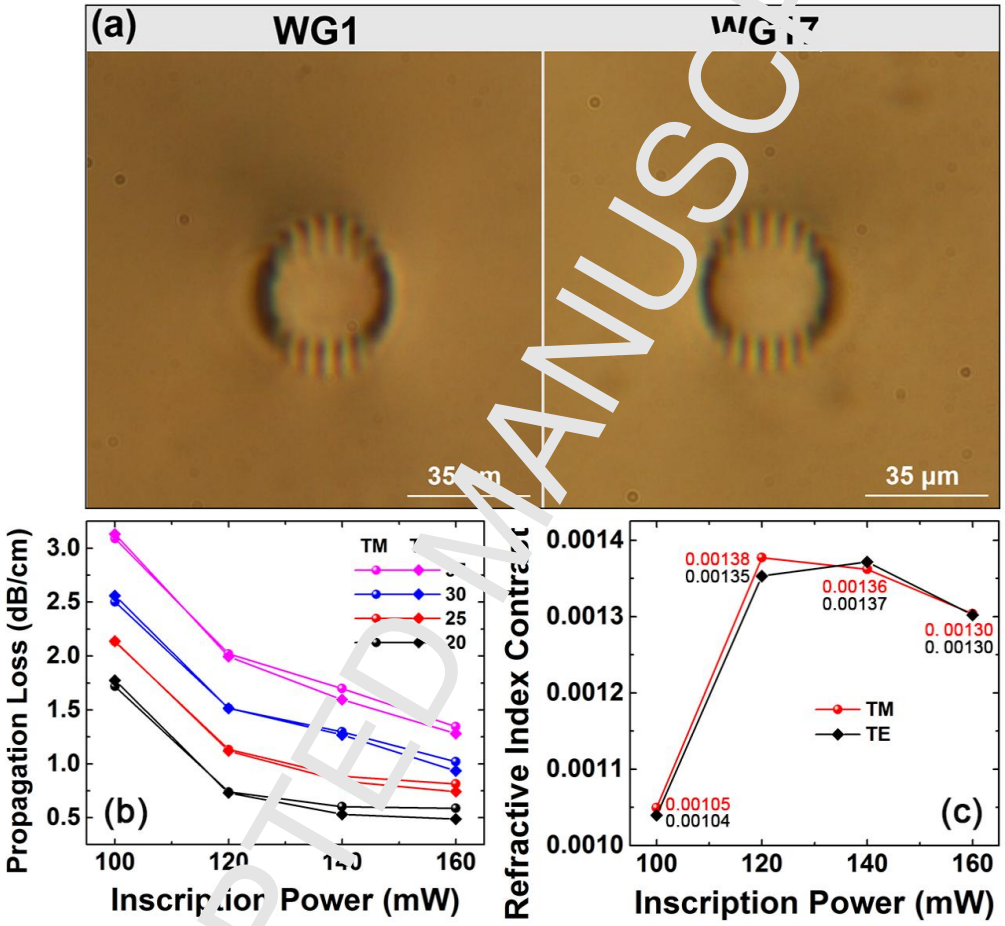

Fig. 1.

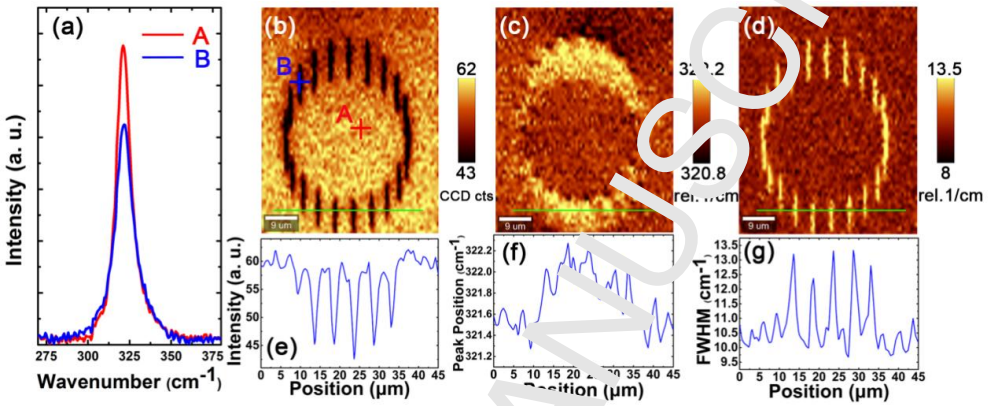

Fig. 2.

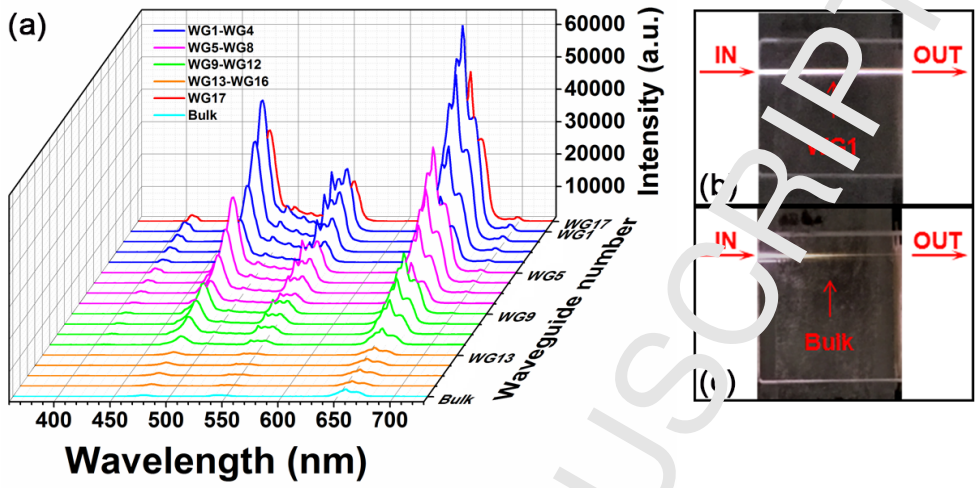

Fig. 3.

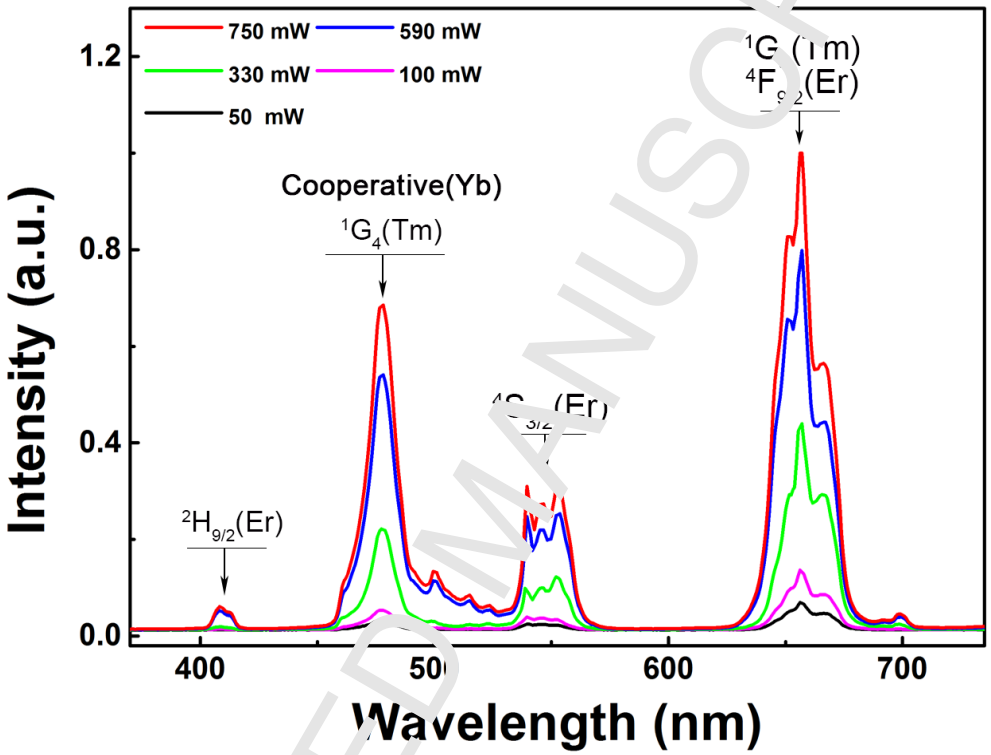

Fig. 4.

Inscription Power (mW) / Diameter (μm)	10 scans				3 scans			
	160	140	120	100	160	140	120	100
35	MM (WG1)	MM (WG5)	MM (WG9)	MM (WG13)	MM (WG17)	MM (WG21)	MM (WG25)	MM (WG29)
30	MM (WG2)	MM (WG6)	MM (WG10)	SM (WG14)	MM (WG18)	MM (WG22)	MM (WG26)	SM (WG30)
25	MM (WG3)	MM (WG7)	MM (WG11)	SM (WG15)	MM (WG19)	MM (WG23)	SM (WG27)	SM (WG31)
20	SM (WG4)	SM (WG8)	SM (WG12)	SM (WG16)	SM (WG20)	SM (WG24)	SM (WG28)	SM (WG32)

Table. 1.